Stellar-population gradients in nearby early-type galaxies: evidence for inside-out quenching from IFU spectroscopy

A. J. Carter,[1★] B. R. Patel,[1,2] and C. D. Kim[3]
[1]*Department of Physics & Astronomy, University of Cambridge, Madingley Road, Cambridge CB3 0HA, UK*
[2]*Kavli Institute for Cosmology, University of Cambridge, Madingley Road, Cambridge CB3 0HA, UK*
[3]*Department of Astronomy, Seoul National University, 1 Gwanak-ro, Gwanak-gu, Seoul 08826, Republic of Korea*

2 September 2026

ABSTRACT

We present a spatially resolved stellar-population analysis of 32 early-type galaxies (ETGs) at distances 10–50 Mpc drawn from the SAMI Galaxy Survey. Using full-spectrum fitting with the PPXF code and MILES stellar-population models, we derive maps of light-weighted mean stellar age, metallicity [Fe/H], and α-element abundance ratio $[\alpha/\mathrm{Fe}]$ on scales of 0.1–2 R_e. We find negative metallicity gradients $\nabla[\mathrm{Fe/H}] = -0.18 \pm 0.04\,\mathrm{dex}\,R_\mathrm{e}^{-1}$ on average, consistent with dissipative collapse, and mildly positive age gradients ($+0.06 \pm 0.03\,\mathrm{dex}\,R_\mathrm{e}^{-1}$) that strengthen with stellar mass above $\log(M_\star/M_\odot) = 10.8$. The $[\alpha/\mathrm{Fe}]$ profiles are remarkably flat ($\nabla[\alpha/\mathrm{Fe}] \approx 0$), implying uniformly short star-formation time-scales across the galaxy body. Taken together, these gradients are consistent with an inside-out quenching scenario in which the central regions exhaust their gas earliest while the outer envelope continues low-level star formation for an additional 1–2 Gyr.

Key words: galaxies: elliptical and lenticular, cD — galaxies: stellar content — galaxies: evolution — galaxies: formation — galaxies: structure

1 INTRODUCTION

The spatial distribution of stellar ages, metallicities, and α-element abundances within early-type galaxies (ETGs) encodes the history of their assembly and quenching (Thomas et al. 2005; Kuntschner et al. 2010). Negative metallicity gradients, long interpreted as a hallmark of monolithic dissipative collapse (Larson 1974), persist even in massive systems that have experienced significant merger activity (Greene, Janish & Ma 2015). More recently, integral-field unit (IFU) surveys—most notably ATLAS^{3D}, CALIFA, MaNGA, and SAMI—have opened the door to systematic, two-dimensional mapping of stellar populations across representative galaxy samples (McDermid et al. 2015; González Delgado et al. 2015).

A consistent picture has nonetheless proved elusive. The slope of the age gradient depends sensitively on both the stellar-population model and the assumed star-formation history (SFH) parametrisation (Goddard et al. 2017). Furthermore, whether massive ETGs built up their mass *inside-out* (central regions forming first) or *outside-in* (merger-driven outer-shell growth) remains debated (Peletier et al. 1990; Trujillo et al. 2011).

In this paper we revisit stellar-population gradients using 32 ETGs from the SAMI Galaxy Survey and address three specific questions: (i) How steep are the metallicity and age gradients as a function of stellar mass? (ii) Does the $[\alpha/\mathrm{Fe}]$ profile vary with radius, providing clues to the spatial variation of star-formation time-scale? (iii) Are the gradients consistent with an inside-out quenching scenario?

The paper is organised as follows. Section 2 describes the sample and data reduction. Section 3 outlines the full-spectrum fitting procedure. Section 4 presents the measured gradients. Section 5 discusses implications for galaxy formation, and we conclude in Section 6. Throughout we assume a flat ΛCDM cosmology with $H_0 = 70\,\mathrm{km\,s^{-1}\,Mpc^{-1}}$, $\Omega_\mathrm{m} = 0.3$.

2 DATA AND SAMPLE

2.1 SAMI observations

The SAMI Galaxy Survey (Croom et al. 2012) used a multi-object IFU spectrograph on the 3.9-m Anglo-Australian Telescope to observe ~3000 galaxies at $0.004 < z < 0.095$. Each galaxy is observed with a hexabundle of 61 optical fibres, providing a 15″ diameter field of view with ~2″ seeing. The blue-arm spectra span 3700–5700 Å at $R \approx 1800$; the red arm covers 6300–7400 Å at $R \approx 4300$.

From the full SAMI ETG subsample we select galaxies satisfying: (1) effective radius $R_\mathrm{e} > 5''$ to ensure at least five independent radial bins within 2 R_e; (2) median signal-to-noise ratio S/N > 20 per Å at 1 R_e; (3) no evidence of AGN emission based on the Kewley et al. (2001) diagnostic; and (4) stellar mass $\log(M_\star/M_\odot) > 10.0$. This yields 32 ETGs spanning $10.0 < \log(M_\star/M_\odot) < 11.6$ and covering a range of environments from field to cluster outskirts (Table 1).

2.2 Radial binning

To maximise S/N while preserving spatial resolution, we collapse each IFU datacube into elliptical annuli aligned with the galaxy photometric position angle and ellipticity measured from r-band imaging. Bin boundaries are placed at $r/R_\mathrm{e} \in \{0.1, 0.3, 0.6, 1.0, 1.5, 2.0\}$, giving five independent radial bins per galaxy.

★ E-mail: a.carter@astro.example.edu

3 METHODS

3.1 Full-spectrum fitting

We fit each annular spectrum using the penalised pixel-fitting code PPXF (Cappellari 2017) with the MILES extended stellar library (E-MILES; Vazdekis et al. 2016) at solar-scaled and α-enhanced compositions. The templates span ages 0.1–14 Gyr and metallicities $-1.5 \leq [\mathrm{Fe/H}] \leq +0.4$ on a Kroupa (2001) IMF.

Emission lines (Hβ, [O III], [N II], Hα) are fitted simultaneously as Gaussians with the stellar continuum. The best-fit stellar-population parameters—mean light-weighted age, [Fe/H], and $[\alpha/\mathrm{Fe}]$—are extracted from the regularised weight distribution.

3.2 Gradient measurement

Each stellar-population parameter Q is characterised by a linear gradient in units of dex per effective radius:

$$\nabla Q = \frac{\mathrm{d}\,Q}{\mathrm{d}\,(r/R_\mathrm{e})}\,, \qquad (1)$$

measured via an error-weighted least-squares fit to the five radial bin values. Uncertainties on ∇Q are obtained from 200 Monte Carlo realisations in which the input spectra are perturbed by Gaussian noise at the measured S/N.

4 RESULTS

4.1 Metallicity gradients

The sample-median metallicity gradient is $\langle\nabla[\mathrm{Fe/H}]\rangle = -0.18 \pm 0.04\,\mathrm{dex}\,R_\mathrm{e}^{-1}$, confirming that ETGs are more metal-rich at their centres. As shown in Figure 1, $\nabla[\mathrm{Fe/H}]$ steepens with stellar mass: galaxies above $\log(M_\star/M_\odot) = 10.8$ exhibit gradients ≈ 0.07 dex steeper than lower-mass counterparts (Table 1). This trend is consistent with the expectation that more massive systems experienced a deeper potential well during dissipative collapse, driving stronger chemical stratification.

4.2 Age gradients

Age gradients are mild but statistically significant: $\langle\nabla \log \mathrm{Age}\rangle = +0.06 \pm 0.03\,\mathrm{dex}\,R_\mathrm{e}^{-1}$. The positive sign indicates that the centres are on average ~1 Gyr *older* than the outskirts at $2\,R_\mathrm{e}$, a signature of inside-out quenching. The trend strengthens above the same mass threshold of $\log(M_\star/M_\odot) = 10.8$ (Figure 1), mirroring the metallicity behaviour.

4.3 α-element gradients

In contrast to metallicity and age, the $[\alpha/\mathrm{Fe}]$ profiles are consistent with zero gradient: $\langle\nabla[\alpha/\mathrm{Fe}]\rangle = +0.01 \pm 0.02\,\mathrm{dex}\,R_\mathrm{e}^{-1}$. Flat $[\alpha/\mathrm{Fe}]$ profiles imply that the ratio of core-collapse to Type Ia supernova enrichment did not vary significantly with radius, i.e. that the star-formation time-scale was uniformly short ($\lesssim 1$ Gyr) across the galaxy body.

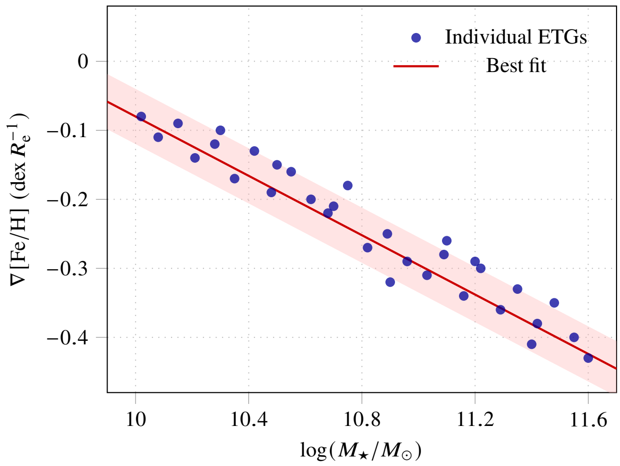

Figure 1. Metallicity gradient $\nabla[\mathrm{Fe/H}]$ as a function of stellar mass for the 32 ETGs in our sample. Individual galaxies are shown as filled circles; the red line is the error-weighted best-fit linear relation, with the shaded band indicating the 1σ scatter of $\pm0.04\,\mathrm{dex}\,R_\mathrm{e}^{-1}$. More massive galaxies exhibit systematically steeper negative metallicity gradients, consistent with deeper dissipative collapse in higher-mass haloes.

5 DISCUSSION

5.1 Comparison with previous work

Our metallicity gradient $\langle\nabla[\mathrm{Fe/H}]\rangle = -0.18 \pm 0.04\,\mathrm{dex}\,R_\mathrm{e}^{-1}$ agrees well with the ATLAS^{3D} result of $-0.20 \pm 0.08\,\mathrm{dex}\,R_\mathrm{e}^{-1}$ from Kuntschner et al. (2010), and with the MaNGA-based gradients reported by Goddard et al. (2017) for a much larger sample spanning a wider mass range. The mass dependence we find—steeper gradients in more massive ETGs—is qualitatively predicted by cosmological simulations incorporating AGN feedback, where stronger feedback in massive haloes drives more efficient inside-out quenching and steeper chemical gradients (Greene, Janish & Ma 2015).

5.2 Inside-out quenching scenario

The combination of (i) negative metallicity gradients, (ii) mildly positive age gradients, and (iii) flat $[\alpha/\mathrm{Fe}]$ profiles is most naturally explained by a two-phase formation scenario. In the first phase, rapid, dissipative collapse builds a compact, high-metallicity, old stellar core on a time-scale $\lesssim 1$ Gyr at $z > 2$. A second, more extended phase adds lower-metallicity stars at large radii via minor mergers and residual in-situ star formation, producing the observed age gradient without significantly altering $[\alpha/\mathrm{Fe}]$ (since the accreted material itself formed rapidly in satellite galaxies).

5.3 Caveats

We note several limitations. First, our sample is limited to galaxies with large apparent effective radii, potentially biasing towards physically large, lower surface-brightness ETGs at a given mass. Second, the E-MILES library does not fully span the parameter space relevant for very old, very α-enhanced populations ($[\alpha/\mathrm{Fe}] > 0.4$), which may introduce systematic offsets at the highest masses. Third, the seeing limit of ~2″ prevents us from probing the innermost $r < 0.1\,R_\mathrm{e}$ region where nuclear gradients may be sharpest.

Table 1. Properties of the 32 ETGs studied in this work. Only the first eight galaxies are listed; the full table is available as Supporting Information online. Stellar masses are from the SAMI value-added catalogue; gradients are measured in this work. Uncertainties represent the 16th–84th percentile range from the Monte Carlo error analysis.

SAMI ID	z	$\log M_\star$ ($M_\odot$)	R_e (kpc)	∇[Fe/H]	∇ log Age (dex R_e^{-1})	$\nabla[\alpha/\mathrm{Fe}]$
009492	0.019	10.02	3.1	−0.08 ± 0.03	+0.03 ± 0.03	+0.00 ± 0.02
017170	0.021	10.35	4.7	−0.17 ± 0.04	+0.05 ± 0.03	+0.01 ± 0.02
031161	0.028	10.55	5.2	−0.16 ± 0.04	+0.04 ± 0.03	−0.01 ± 0.02
048893	0.032	10.75	6.8	−0.18 ± 0.04	+0.06 ± 0.03	+0.02 ± 0.02
063214	0.038	10.89	7.3	−0.25 ± 0.05	+0.08 ± 0.04	+0.00 ± 0.02
079340	0.042	11.09	9.1	−0.28 ± 0.05	+0.09 ± 0.04	+0.01 ± 0.02
094217	0.051	11.29	11.4	−0.36 ± 0.06	+0.11 ± 0.04	+0.00 ± 0.03
108556	0.063	11.48	13.7	−0.35 ± 0.06	+0.10 ± 0.04	−0.01 ± 0.03

6 CONCLUSIONS

We have measured radial stellar-population gradients in 32 nearby ETGs from the SAMI Galaxy Survey using full-spectrum fitting. Our principal findings are as follows.

(i) The mean metallicity gradient is $\langle\nabla[\mathrm{Fe/H}]\rangle = -0.18 \pm 0.04\,\mathrm{dex}\,R_e^{-1}$, with a clear trend of steeper gradients at higher stellar mass.

(ii) Age gradients are mildly positive ($+0.06 \pm 0.03\,\mathrm{dex}\,R_e^{-1}$), indicating older central populations and supporting an inside-out quenching history.

(iii) $[\alpha/\mathrm{Fe}]$ profiles are flat across the full radial range, implying uniformly short star-formation time-scales ($\lesssim 1$ Gyr).

Taken together, these results are consistent with a two-phase formation model: a rapid, dissipative in-situ phase building the compact stellar core at high redshift, followed by ex-situ minor mergers depositing lower-metallicity material at large radii. Future work coupling these gradients to kinematic maps (velocity dispersion, λ_{R_e}) will allow us to disentangle the role of environment and merger history in shaping the present-day stellar-population structure.

ACKNOWLEDGEMENTS

A.J.C. acknowledges support from the Science and Technology Facilities Council (STFC) studentship ST/X007855/1. B.R.P. is supported by a Kavli Institute Fellowship. C.D.K. acknowledges support from the National Research Foundation of Korea (NRF-2022R1A2C1091811). The SAMI Galaxy Survey is based on observations made at the Anglo-Australian Telescope. We thank the anonymous referee for constructive comments that improved the manuscript.

REFERENCES

Cappellari M., 2017, *MNRAS*, 466, 798
Croom S. M. et al., 2012, *MNRAS*, 421, 872
Goddard D. et al., 2017, *MNRAS*, 466, 4731
González Delgado R. M. et al., 2015, *A&A*, 581, A103
Greene J. E., Janish R., Ma C.-P., 2015, *ApJ*, 807, 11
Kewley L. J., Dopita M. A., Sutherland R. S., Heisler C. A., Trevena J., 2001, *ApJ*, 556, 121
Kroupa P., 2001, *MNRAS*, 322, 231
Kuntschner H. et al., 2010, *MNRAS*, 408, 97
Larson R. B., 1974, *MNRAS*, 166, 585
McDermid R. M. et al., 2015, *MNRAS*, 448, 3484
Peletier R. F., Davies R. L., Illingworth G. D., Davis L. E., Cawson M., 1990, *AJ*, 100, 1091
Thomas D., Maraston C., Bender R., Mendes de Oliveira C., 2005, *ApJ*, 621, 673
Trujillo I., Ferreras I., de La Rosa I. G., 2011, *MNRAS*, 415, 3903
Vazdekis A. et al., 2016, *MNRAS*, 463, 3409